Chapter 1

Introduction

1.1 Motivation

Flow-induced vibration in shell-and-tube heat exchangers has been studied for more than 40 years. More intensified efforts for the prediction of failure in shell-and-tube heat exchangers are being made because of the cost associated with premature failure. Several phenomena associated with flow-induced vibration exist. These include fluid-elastic instability, acoustic resonance, vortex shedding, turbulence buffeting and parallel-flow eddy formation. Tube vibration is not only caused by the excitation frequencies associated with the above mentioned phenomena, but also by motion dependent fluid forces, which are in turn caused by tube vibration, as described by Goyder and Whalley (1987).

Sasol Synthetic Fuels (SSF) uses more than two thousand shell-and-tube heat exchangers in their processes. In a never-ending quest for excellence, plant production capacities is ever increasing. This often leads to the operation of equipment, including shell-and-tube heat exchangers, above their intended design limits. Because shell-and-tube heat exchangers are susceptible to flow-induced vibration, vibration analyses are required in such instances. Several assessment methods exist, as described in the Heat Exchanger Design Handbook HEDH (1998) and Tubular Exchangers Manufacturing Association TEMA (1988). These methods are used in software such as the Heat Transfer and Fluid Flow Services HTFS (1992) and the Heat Transfer Research Institute HTRI packages. These methods however, use large margins of uncertainty (in the order of 20 percent) for the prediction of flow-induced vibration. Because of the high replacement cost of heat exchangers, additional methods are required to predict and verify vibration problems and the extent thereof.

Numerous vibration experiments have been conducted under controlled conditions, using single tubes or ideal tube banks exposed to uniform cross-flow or parallel-flow velocities. Very few investigations have addressed the specific problems associated with industrial heat exchanger configurations. The application of results from ideal test conditions is often difficult, because of

differences in geometry, in the way the flow is coupled to the motion of the tubes, and in the non-uniformity of the velocities throughout the bundle. Consequently, the ability to accurately predict the intensity of flow-induced vibration, or the probability of damage, is less than certain (Chenoweth, 1998).

1.2 Literature study: Flow-induced vibration

In the literature study the tube bundle vibration and natural frequencies will be described, followed by the mechanisms that cause tube vibration and the failures associated with excessive vibration. The literature study also includes a case study of a shell-and-tube heat exchanger that failed during operational conditions. Four heat exchanger vibration studies from Sasol are also included in the case study.

1.2.1 Tube bundle vibration

The natural frequency of a tube is dependent on the material properties, span length, geometry and supports.

Natural frequencies of straight tubes

In a shell-and-tube heat exchanger it is adequate to determine the lowest frequency only. If assuming that the tubes are fixed at the tubesheets and simply supported at the baffles with equal span length between the baffles, the following approach by Chenoweth (1998) can be used:

$$f_n = \frac{C_n}{2\pi}\left(\frac{EI}{M_e L^4}\right)^{0.5} \qquad 1.1$$

where the effective mass per unit length (M_e) can be determined as described by TEMA. Values for C_n are given in figure 1.1. E, I and L are the modulus of elasticity, second moment of area and unsupported tube length respectively. Most heat exchangers have their longest unsupported span length passing through the baffle window or in the entrance or exit zones. It is therefore necessary to determine the lowest natural frequency by considering all the possible combinations as described in figure 1.1.

A further aspect to consider is the effect of axial stresses, which may be caused by manufacturing procedures or operating conditions like thermal expansion. If

the axial force (P_a) is known, the natural frequency can be modified using the following relationship:

$$f_{ns} = f_n\left(1+\frac{P_a L^2}{EI\pi^2}\right)^{0.5} \qquad 1.2$$

If the axial force is compressive, the sign of P_a is negative and the natural frequency decreases. The variation in natural frequency due to axial forces may be as much as 40 percent, as described by Kissel (1972). Tube to baffle hole clearances have little effect on the natural frequency but are important when considering the amount of damping and tube wear.

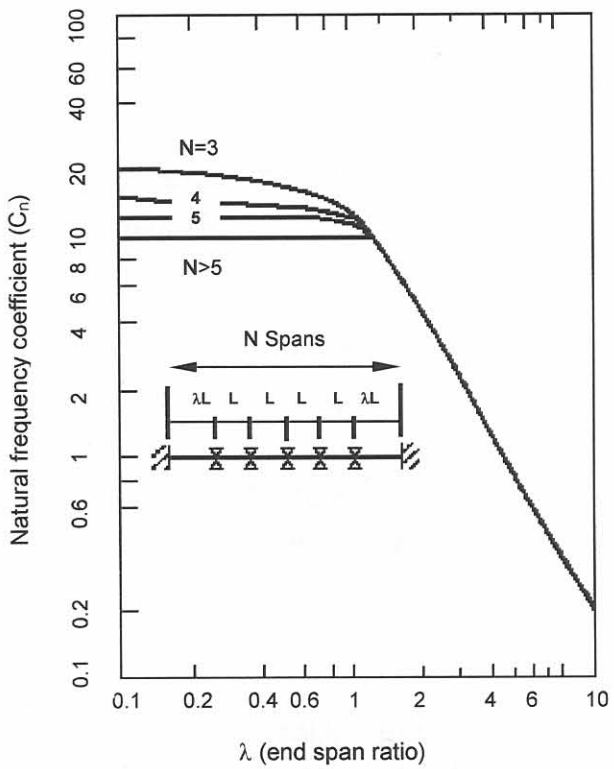

Figure 1.1: Straight tube natural frequency coefficients (Chenoweth, 1998)

Natural frequencies of U-tubes

TEMA uses equation 1.3 to obtain the lowest natural frequency:

$$f_{nu} = 59.55\frac{C_u}{R^2}\left(\frac{EI}{M_e}\right)^{0.5} \qquad 1.3$$

Where R is the U-tube radius. Values for C_u for different support configurations can be obtained, as described by the TEMA specifications.

Finned-tube natural frequencies

Finned-tube natural frequencies can be determined using equation 1.1, if the second moment of area (I) in the equation is calculated using an effective diameter and the mass per unit length is taken as the actual mass of the finned section. This is only true if the finned-tubes enter the baffles in such a manner that the assumption of simple supports is satisfied.

1.2.2 Damping

The amplitude of vibration is strongly dependent on the damping of the system. The following equations for logarithmic decrement, (δ) given by TEMA, are based on idealised models and experimental observations. For shell side liquids δ is equal to the greater of δ_1 or δ_2:

$$\delta_1 = \frac{3.41 d_o}{w_o f_n} \tag{1.4}$$

$$\delta_2 = \frac{0.012 d_o}{w_o}\left[\frac{\rho_o v}{f_n}\right]^{0.5} \tag{1.5}$$

For shell side vapours:

$$\delta = \frac{0.314(N-1)}{N}\left[\frac{t_b}{l}\right]^{0.5} \tag{1.6}$$

where w_o is the effective weight in lb, ρ_o is the density of the shell side fluid in lb/in^3 and d_o (inches) is the outside diameter of the tubes. For calculating the damping for vapours, the baffle plate thickness (t_b), length (l) and the number of spans (N) are used in equation 1.6. For two-phase flow cases see Kawamura *et al.* (1997) and Gidi *et al.* (1997).

1.2.3 Fluid forces

Fluid forces can be divided into fluid excitation forces (figure 1.2) and motion-dependent fluid forces (Chen, 1991 and 1992).

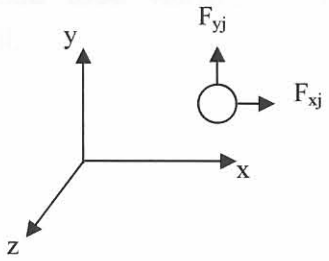

Figure 1.2: Tube force directions

Fluid excitation forces:

$$F_{xj} = \frac{1}{2}\rho U^2 DC_{Dj} + \frac{1}{2}\rho U^2 DC_{Dj}^{'} \sin(\Omega_{Dj} + \Phi_{Dj}) + g_j^{'} \qquad 1.7$$

$$F_{yj} = \frac{1}{2}\rho U^2 DC_{Lj} + \frac{1}{2}\rho U^2 DC_{Lj}^{'} \sin(\Omega_{Lj} + \Phi_{Lj}) + h_j^{'} \qquad 1.8$$

where D is the diameter of the cylinder and U is the flow velocity. C_D and C_L are the steady drag and lift coefficients with $C_D^{'}$ and $C_L^{'}$ the fluctuation of the coefficients. Ω is the circular frequency of periodic flow with Φ the corresponding phase angle with respect to a particular fluid-force component. $h^{'}$ and $g^{'}$ represent other fluctuating forces such as turbulent buffeting forces.

Motion-dependent fluid forces:

$$F_{xj} = -\sum_{k=1}^{N}\left[\left(\bar{\alpha}_{jk}\frac{\partial^2 u_k}{\partial t^2} + \bar{\alpha}_{jk}^{'}\frac{\partial u_k}{\partial t} + \bar{\alpha}_{jk}^{''}u_k\right) + \left(\bar{\sigma}_{jk}\frac{\partial^2 v_k}{\partial t^2} + \bar{\sigma}_{jk}^{'}\frac{\partial v_k}{\partial t} + \bar{\sigma}_{jk}^{''}v_k\right)\right] \qquad 1.9$$

$$F_{yj} = -\sum_{k=1}^{N}\left[\left(\bar{\tau}_{jk}\frac{\partial^2 u_k}{\partial t^2} + \bar{\tau}_{jk}^{'}\frac{\partial u_k}{\partial t} + \bar{\tau}_{jk}^{''}u_k\right) + \left(\bar{\beta}_{jk}\frac{\partial^2 v_k}{\partial t^2} + \bar{\beta}_{jk}^{'}\frac{\partial v_k}{\partial t} + \bar{\beta}_{jk}^{''}v_k\right)\right] \qquad 1.10$$

where $\bar{\alpha}_{jk}$, $\bar{\beta}_{jk}$, $\bar{\tau}_{jk}$ and $\bar{\sigma}_{jk}$ are added mass matrices; $\bar{\alpha}_{jk}^{'}$, $\bar{\beta}_{jk}^{'}$, $\bar{\tau}_{jk}^{'}$ and $\bar{\sigma}_{jk}^{'}$ are damping matrices, $\bar{\alpha}_{jk}^{''}$, $\bar{\beta}_{jk}^{''}$, $\bar{\tau}_{jk}^{''}$ and $\bar{\sigma}_{jk}^{''}$ are fluid stiffness matrices and subscript j and k indicates the tube position.

1.2.4 Excitation mechanisms for tube vibration

It is possible that vibration can be transmitted from an external source to the heat exchanger through foundations or supporting structures. This research, however, is limited to flow-induced tube vibration. The following mechanisms will be discussed in more detail:

- Fluid-elastic instability
- Vortex shedding
- Acoustic resonance
- Turbulence buffeting
- Flow pulsation
- Parallel-flow eddy formation

Fluid-elastic instability

Chenoweth (1998) characterises Fluid-Elastic Instability (FEI) as a whirling type of tube vibration with the tube deflection moving orbitally. Flow across the tubes produces a combination of drag and lift forces. Brenneman and Gurdal (1997) describes the fluid elastic mechanism in tube bundles as a simple first-order mechanism that is proportional to the dynamic pressure in the fluid flowing between the tubes and inversely proportional to the zero-crossing frequency of the relative tube responses. Fluid-elastic instability is important in both liquids and gasses. If the fluid velocity is above the critical velocity, a drastic increase in vibration amplitude will occur (figure 1.3).

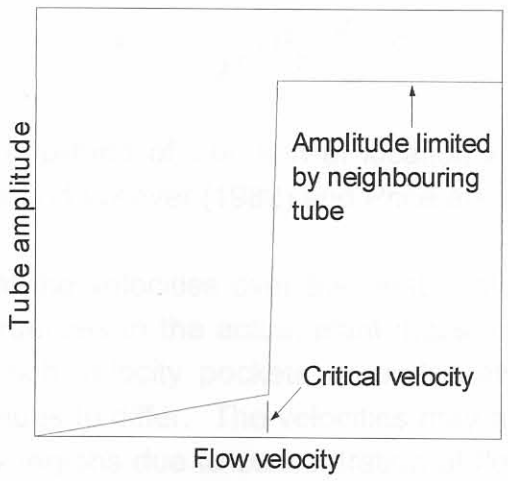

Figure 1.3: Variation of tube amplitude with flow velocity (HTFS).

Goyder (1997) examined the margins of uncertainty in which FEI in heat exchanger tube bundles can be predicted and the actual occurrence of damaging vibration. The following inequality for assessing the stability of a tube bundle is given by Goyder (1997):

$$\frac{2\pi\zeta_n m_n}{\rho_o D^2} > \int_0^L \frac{\rho(z)}{\rho_o}\left[\left(\frac{U_g}{f_n D}\right)^2 \frac{C}{8\pi}\right]\frac{\Phi_n^2(z)}{I_n}dz \qquad 1.11$$

The inequality must be satisfied for stability. C is the fluid force coefficient and Φ is the mode shape. ξ_n and m_n are the damping and mass at the nth natural frequency. The gap flow velocity (U_g) is defined by:

$$U_g = \frac{G}{\rho A}\left(\frac{P}{P-D}\right) \qquad 1.12$$

The mode shapes can broadly be classified in two categories. Firstly tubes with a relatively long end span where most of the vibration occurs. In this case the end spans may be treated as single span tube bundles and the mid-spans may be ignored. Alternatively the end spans may be relatively short. In this case the tube can be modelled as a set of equally spaced mid spans with an approximate mode shape. The end-span length is taken equal to the mid-span length.

$$\Phi(x) = \sin\left(\frac{\pi x}{NL_{mid}}\right)\sin\left(\frac{\pi x}{L_{mid}}\right) \qquad 1.13$$

The forces associated with the gap flow velocity are given in terms of the fluid force coefficient C, which relate the force to the amplitude of vibration.

$$F(x) = \frac{1}{2}\rho U_g^2 D\frac{a(x)}{D}C \qquad 1.14$$

where $a(x)$ is the amplitude of vibration at location x. Values for C have been developed by Lever and Weaver (1982) and Price and Paidoussis (1984).

The problem is that the velocities over the heat exchanger tube bundle are not well known. Uncertainties in the actual plant mass flow rate, gas density, cross flow fraction and high velocity pockets around sealing strips, may cause the nominal velocity values to differ. The velocities may also be different because of nozzle and window regions due to concentration of flow. The influencing factors have a typical uncertainty value of 20 percent. In a turbulence, stability and wear

analysis of a steam generator, Brenneman and Gurdal (1997) showed that the critical fluid-elastic velocity is only a weak function of the tube-to-baffle clearances.

Kassera (1997) analysed a single elastically mounted tube in cross flow with a three-dimensional Computational (CFD) code as shown in figure 1.4. Results were obtained for rigid and vibrating tubes. When the vibrations of the tubes are taken into account, much better correlation with experimental data is obtained.

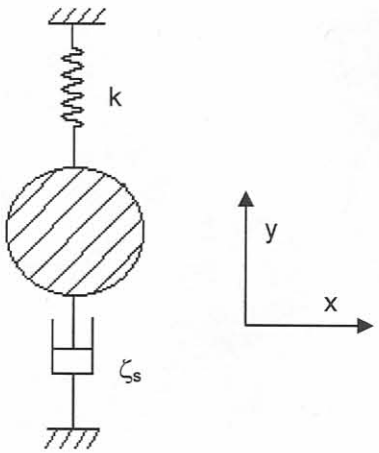

Figure 1.4: Spring and dashpot system used by Kassera (1997)

To calculate the flow-induced vibration (vibrating tubes) first, the flow field is calculated using a CFX (Reynolds-stress model). The drag and lift loads can then be determined and used to calculate the velocity and displacement of the tube. The grid is then recalculated because of the displacement of the tube and the tube velocity is taken as a new boundary condition for the next time step.

Chen *et al.* (1997) describe a direct-measurement technique for determining the fluid damping and fluid stiffness coefficients that are given in section 1.2.3. Chen *et al.* concluded that fluid-damping-controlled instability is most likely associated with the motion in the lift direction because in many cases $\vec{\alpha}$ is positive while $\vec{\beta}$ is negative (equations 1.9 and 1.10).

Vortex shedding

Vortex shedding is the principal excitation mechanism for flow-induced vibration in cross flow, producing alternating forces, which occur more frequently if the flow

velocity is increased (figure 1.5). Vortex shedding is fluid-mechanical in nature and does not depend on the movement of the tubes.

If the vortex shedding frequency (equation 1.15) and one of the tube's natural frequencies differ by less than 20 percent, 'lock in' may occur. 'Lock in' is a phenomenon whereby the vortex shedding frequency changes to become exactly equal to one of the tube's natural frequencies. The vortex shedding frequency is a function of the Strouhal number (Sr), velocity and the diameter (D_o) of the tubes as shown in equation 1.15

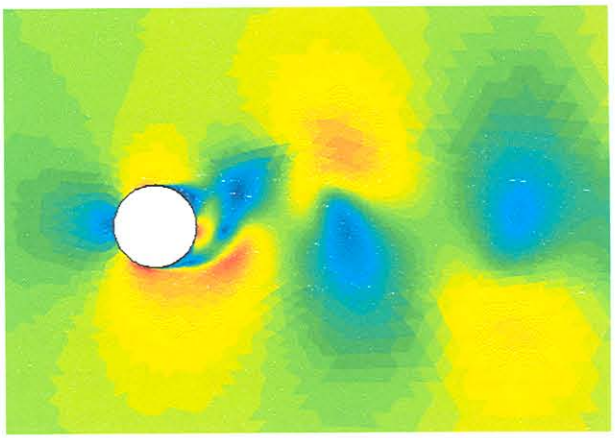

Figure 1.5: Vortex shedding: Single cylinder in cross flow

$$f_{vs} = \frac{S_r u}{D_o} \qquad 1.15$$

Studies showed that the Strouhal numbers in tube arrays are functions of Reynolds number and that there are multiple Strouhal numbers at a given Reynolds number. Chen (1968) and Fitz-Hugh (1973) developed Strouhal number correlations. These correlations contain some inconsistencies. Oengören and Ziada (1997) showed that Strouhal number data grouped mainly around different Strouhal number lines (see figure 1.6). Xp is the tube pitch to diameter ratio.

Vortex shedding forces in liquids are usually sufficiently large (if the natural frequency of tubes is close to the vortex shedding frequency) to produce tube vibration. In gases, vortex shedding is only important if the tube damping is small or the gas has a high density or large velocity (Chen, 1992).

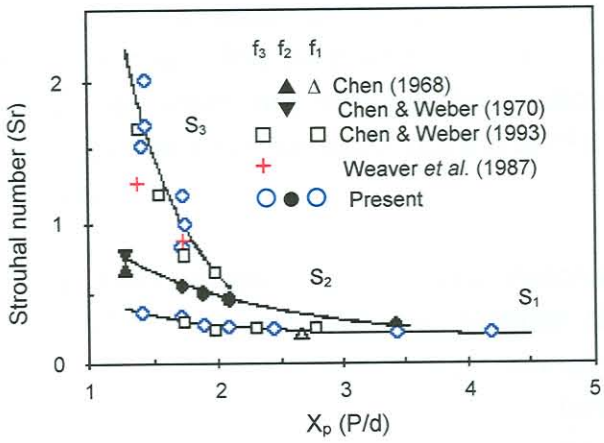

Figure 1.6: Strouhal number chart (Oengören and Ziada, 1997).

Acoustic resonance

Acoustic vibration only occurs when the shell-side fluid is a vapour or a gas. Two types of frequencies can be associated with acoustic vibration: Acoustic frequency (f_a) of the heat exchanger and the acoustic wake-shedding frequency of the tube bundles (f_s). When these two frequencies coincide, acoustic resonance can occur. Acoustic resonance can only lead to vessel and vessel support damage if this resonance frequency matches the natural frequency of the tubes. HTFS suggests the following criteria:

For a cylindrical geometry, if the frequency ratio is within 20 percent (equation 1.16)

$$0.8 < \frac{f_a}{f_s} < 1.2 \qquad 1.16$$

then acoustic resonance may be generated (where f_a is the acoustic frequency and f_s is the acoustic wake-shedding frequency).

If acoustic resonance 'lock in' occurs and if the natural frequency is within 20 percent of the shedding frequency (eq. 1.17)

$$0.8 < \frac{f_n}{f_s} < 1.2 \qquad 1.17$$

then tube vibration may occur (where f_n is the fundamental frequency of the tube). HTFS (1992) gives a more detailed discussion on how to determine the frequencies described above. The problem is that the speed of sound and the acoustic Strouhal number, which are used in these calculations, are difficult to obtain. Strouhal number maps can be used, but the errors may be in the order of 25 percent (HTFS, 1992).

Oengören and Ziada (1997) investigated acoustic resonance in triangular tube bundles and developed an acoustic Strouhal number chart. This chart was developed using measurements obtained in wind tunnel tests, as well as data from the literature (see figure 1.7). Their study further showed that the mechanism of acoustic resonance in parallel triangle arrays are similar to that of in-line arrays because of the similar free flow lanes between the tubes through which the flow proceed.

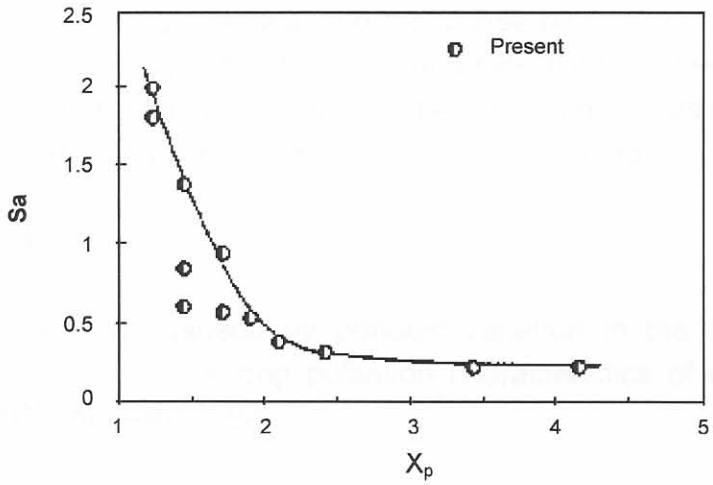

Figure 1.7: Acoustic Strouhal number chart (Oengören and Ziada).
(S_a-acoustic Strouhal number, X_p-tube pitch)

Turbulence buffeting

Turbulent flow contains a wide spectrum of frequencies distributed around a central dominant frequency (see figure 1.8). This frequency increases as the cross flow velocity increases.

Energy dissipation in turbulent flow occurs both because of molecular viscosity and 'turbulent viscosity'. The tube responds easily to an oscillation force at one of its natural frequencies. Chenoweth (1998) gives the following equation (equation 1.18) for determining the turbulent buffeting frequency (f_{tb}):

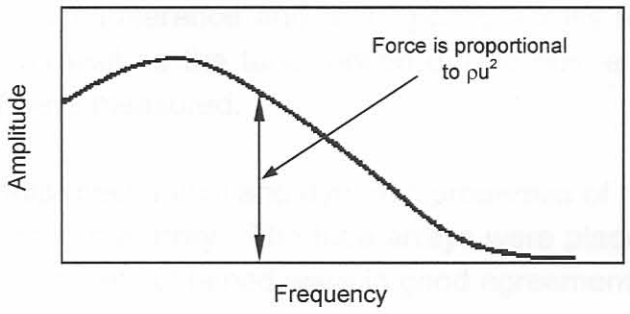

Figure 1.8: Frequency spectrum of the excitation force (HTFS)

$$f_{tb} = \frac{u_c D_o}{p_l p_t}\left[3.05\left(1-\frac{D_o}{p_t}\right)^2 + 0.28\right] \qquad 1.18$$

where p_l and p_t are the longitudinal and transverse pitch of the tube bundle. This equation can only be applied when the shell side fluid is gaseous. The forces associated with turbulent buffeting can be obtained by using fluid structure interaction programs. This process is very time consuming.

Flow pulsation

Tube vibration can be caused by periodic variation in the flow, for example reciprocating machines or strong pulsation characteristics of certain two-phase flow patterns (Chenoweth, 1998).

Parallel-flow eddy formation

Eddies developing along the tube due to parallel-flow can cause vibration. Nuclear reactors and associated heat exchangers have experienced this type of vibration. They typically have very high axial velocities and long unsupported tube spans. Vibration occurs when the velocity reaches a critical value. Methods for determining the critical value are described by Chen and Weber (1970) and Kawamura *et al.* (1997).

1.2.5 Measurements and testing

Romberg and Popp (1997) used a pressure test tube (figure 1.9) to determine the forces acting on a single tube in a bundle subjected to cross-flow random

excitation. The tube provided non-stationary pressure distribution simultaneously at 30 points on the circumference and at 15 points across the tube span. The acting fluid forces as well as the tube motion due to fluid-elastic instability and turbulent buffeting were measured.

The geometrical, fluid-mechanical and dynamic properties of the test tube are the same as other tubes in the array. The tube arrays were placed in a wind tunnel. Some of the measurements obtained were in good agreement with the calculated values.

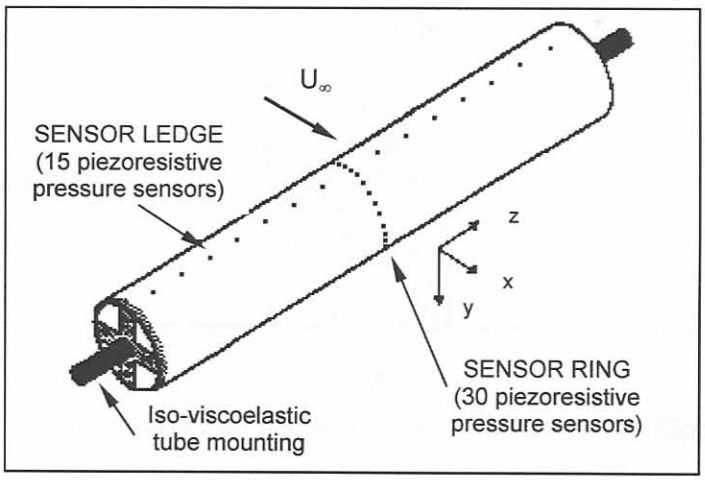

Figure 1.9: Test tube (Romberg and Popp, 1997)

Soper (1980) measured the amplitude of selected tubes (see figure 1.10) using resistance strain gauges bonded to the tube at the maximum bending strain position. These tests were done for four tube configurations. The tests showed that the rotated triangular configuration was the most prone to fluid elastic instability, while the rotated square geometry exhibited the greatest resistance. Intense acoustic standing waves were present in the rotated square geometry, making them unsuitable for applications with gas as a shell-side fluid.

Oengören and Ziada (1997) measured sound pressure levels by condenser microphones located in the tube bundle, subjected to a wind tunnel test. Inada *et al.* (1997) determined the motion-dependent fluid forces by using a tube excitation mechanism and measuring the response of the surrounding tubes.

Hartlen and Anderson (1980) used pre-operational vibration measurements to determine whether or not flow-induced vibration will occur. The tests were conducted with the tubesheet exposed for probe access. A microphone-in-tube technique was used to determine a zone of impacting along with a bi-axial accelerometer probe, which identified the tubes with the highest levels of impacting-accelerations at the baffle and mid-span locations. The vibratory displacement as a function of position, was also measured using the probe.

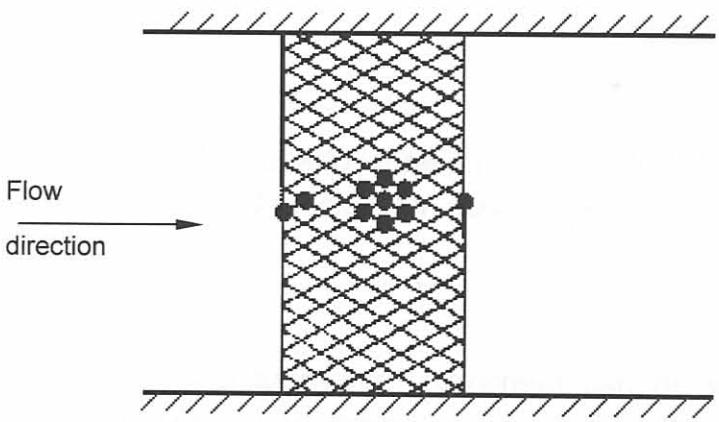

Figure 1.10: Position of instrumented tubes in the tube bundle (Soper, 1980).

1.2.6 Failure and wear

Failure and/or wear in heat exchangers can be caused by:

- Vibration
- Thermal expansion
- Environmental effects

Vibration failure

Mechanical failure of tubes is usually the result of one of the following (as discussed in HEDH (1998)):

a) Collision damage

When the amplitude of vibration is sufficiently large, adjacent tubes collide with one another or with the shell. Collision damage produces a diamond-shape wear

pattern (usually in the mid-span between baffles) where the tube wears thin and eventually splits open.

b) Baffle damage

Baffle hole clearances as given by TEMA, are used to facilitate exchanger bundle assembly. The tubes are therefore not rigidly fixed but can move relative to the baffle. The movement wears the vibrating tubes thin, particularly when the baffles are thin and made of a harder material than the tube.

c) Fatigue

Repeated bending of the tubes due to vibration can lead to failure if the stresses are high enough. Corrosion and erosion can accelerate this process.

d) Tube joint leakage

The tube joints between the tubes and tubesheet can be welded or rolled, causing stress concentrations where the tubes emerge from the tubesheet. Flow-induced vibration may cause leakage between the joints, particularly in fixed shell-and-tube designs where thermal stresses are also induced in the joints.

Thermal expansion

In fixed tubesheet exchangers the tubes are restrained from free thermal expansion. These exchangers are designed so that no expansion joints are needed at normal operating conditions. Problems most often occur during startup, shutdown or some process upset. Floating-head exchangers are not inherently immune to differential expansion problems. In multiple tube passes the temperature difference between adjacent tube passes can cause destructive stresses.

Environmental effects

Corrosion, erosion and fretting reduce the thickness of the tube material. It is therefore necessary to design heat exchangers with a corrosion allowance. Raj *et al.* (1999) examined two cases where corrosion caused failure in heat exchangers.

1.2.7 Case studies

Literature

Hartlen and Anderson (1980) examined heat exchanger failures in a large electricity generating utility, over a period of ten years. The initial failures appear over a widely varying time scale from commissioning up to 15 years of service. In most cases the same failure recurred within a few years. Four cases showed that the failure was caused by fatigue due to high velocities at inlet or outlet regions. In seven cases baffle damage occurred because of acoustic vibration, flow pulsation and maldistribution of shell-side flow. One case of collision damage, corrosion failure and faulty manufacturing occurred. Hartlen and Anderson also describe a pre-operational vibration test that provide commissioning and maintenance information.

Escoe (1997) studied an inadequate flow-induced vibration design of a steam condenser. The condenser exchanger experienced both fluid-elastic instability and turbulence buffeting. The first failure occurred within six months of operation caused by FEI. After fixing this problem, the exchanger failed (tube-to-tube collision) due to low cycle fatigue after 12 years when the shell-side velocity was increased. The exchanger was replaced by a RODbaffle exchanger.

Frick (1997) introduced an empirical Wear Projection Technology (WPT) which relies on data from two or more time independent wear related measurements at a wear site. The WPT method is independent of the wear mechanism and the assessment of ongoing wear is based on projection using constant volume-wear-rate assumptions. The fretting wear damage of an exchanger is proportional to the work-rate (dynamic interaction between the vibrating tube and its supports). Yetiser *et al.* (1997) derived an estimated work-rate formula to predict fretting wear, using turbulence as excitation only. Rao *et al.* (1997) suggested a wear methodology to predict tube wear at scheduled inspections by determining a set of wear parameters from a non-linear finite element simulation, using both FEI and flow induced turbulence as excitation mechanisms. In most operating conditions the range of values for these parameters can vary to quite an extent, therefore deterministic methods were developed to determine the work-rate (Sauvé *et al.*, 1997).

Heat exchangers at Sasol

The heat exchanger that was selected, analysed and measured in Chapters 2, 3, and 4 was from Sasol Synthetic Fuels (SSF). It was therefore also necessary to obtain vibration and failure information from SSF. Four case studies were received from SSF and in all four cases the heat exchangers were TEMA class R.

- 1st Stage raw gas exchanger (12 ES 101)
- Circulating methanol cooler (212 ES 106)
- Main wash methanol cooler (212 ES 158)
- CEU 1000/5600 Horizontal type exchanger (ES 103)

a) 1st Stage raw gas exchanger (12 ES 101)

The raw gas exchanger is a BEM type exchanger with pure gas as shell-side fluid and raw gas as tube-side fluid. A vibration analysis was done to determine whether the shell-side fluid velocity could be increased. Although the analyses from LURGI and SASTECH differed in some respects, the general conclusion was that the probability of acoustic resonance was very high. It was therefore suggested that the exchanger should not be operated at increased flow.

b) Circulating methanol cooler (212 ES 106)

The exchanger is classified as an AKL (tube length 10360 mm) fixed tubesheet exchanger with 2 tube passes, with refrigerant as shell side fluid and loaded methanol as tube side fluid. A vibration analysis with increased load on the shell side was done by LURGI, concluding that there was no risk of acoustic vibration and that vortex shedding was unlikely to occur. LURGI further suggested that the number of baffles be increased from 6 to 7 to shorten the unsupported tube length. Since major repairs would have had to be done to access the bundle, Sasol increased the load without increasing the number of baffles. Vibration measurement on the exchanger was done while operating at higher load which indicated possible vibration of the tubes. The vibration, however, decreased with increased load.

c) Main wash methanol cooler (212 ES 158)

The main wash methanol cooler is also an AKL fixed tubesheet exchanger, with a tube length of 9145 mm. At increased loads, a vibration analysis showed a center vortex shedding ratio of 1.415, which was outside the HTFS range. The

concern was that the shedding frequency passed through the natural tube frequency and that the vibration was not damped out at 1.4 times the natural frequency. Vibration measurements were taken at the increased load condition, without any modifications made to the exchangers and the results were satisfactory.

d) CEU 1000/5600 Horizontal type exchanger (ES 103)

This single pass U-tube exchanger with a rotated square tube array was analysed with increased shell-side flow, using HTFS. The analysis predicted turbulence buffeting and vortex shedding. As rotated square arrays are prone to acoustic resonance, an alternative layout was recommended. The design was changed from having 10 double segmental baffles (21 percent cut) to 6 single segmental (15 percent cut) baffles. This could easily be done, because the exchanger had a floating head tubesheet.

1.3 Scope of the work

The problem of flow-induced vibration in shell-and-tube heat exchangers can be divided into two parts. Firstly, will vibration occur at the increased flow rate? And secondly, will that vibration be sufficiently large to cause failure? The literature study gives an overview of both these problems. Only the first question will be addressed in this research. It is after all more important to first determine whether vibration will occur at increased capacity. Once this question is answered, the amplitude of the vibration and the associated failure modes can be addressed. This second part is therefore not included in the scope of this research.

In the literature study (paragraph 1.2.4) the different mechanisms associated with flow-induced vibration and the corresponding margins of uncertainty, were described. The HTFS software that is used by SASOL, makes use of a 20 percent margin of uncertainty. If a vibration calculation is done on a heat exchanger and the results indicate that the frequencies are just within the 20 percent uncertainty range, does the heat exchanger need to be replaced or are there other methods to determine if vibration will actually occur? The fluid-elastic instability, vortex shedding and turbulence buffeting frequencies are all functions of the flow velocity through the heat exchanger. The margins of uncertainty can therefore be reduced if a more accurate prediction of the flow velocity through the heat exchanger can be obtained. One such method is using a CFD analysis to simulate the flow patterns. CFD analyses are expensive and methods for

reducing the number of analyses are also investigated. This, however, is of no use if the natural frequencies of the tubes are not accurately predicted. The natural frequencies of the tubes (paragraph 1.2.2) can vary with as much as 40 percent, depending on the axial forces in the tube. Additional measurements to determine the natural frequencies of the tubes are also needed.

The objective of this research is to verify existing flow-induced vibration prediction methods by using CFD analyses and experimental work and to obtain a more accurate prediction of flow-induced vibration when the heat exchangers is within the uncertainty range to determine if the heat exchanger life can be extended .

1.4 Research Methodology

To combine the methods for the prediction of flow-induced vibration, the following steps were taken as shown in figure 1.11.

First a HTRI or HTFS analysis on the heat exchanger is performed. If the vibration frequencies obtained from the analysis are within the 20 percent uncertainty range, CFD analyses and experimental vibration measurement are required. The HTRI calculated frequency is then compared to the experimentally measured frequency where vibration in the heat exchanger occurred. The measured velocities at which vibration occurred in the heat exchanger, are also compared to the HTRI and CFD predicted values. If the mass flow rate falls within the predicted frequency range where vibration will occur, additional methods such as fluid structure analyses are required. If the increased mass flow rate falls outside the frequency range, the heat exchanger can be operated successfully at increased mass flow rates.

1.5 Layout

In Chapter 2 a heat exchanger at SSF is selected that complied with the specified criteria. The flow rates at which vibration problems are likely to occur, are determined using HTRI software. FEM analyses are also performed to confirm the natural frequencies, as calculated by the HTRI analyses. Additional higher natural frequencies are also obtained from this process. The flow through the heat exchanger is analysed in Chapter 3 using Computational Fluid Dynamics

simulations (CFD). From these analyses the average cross-flow velocities and pressure drop through the selected heat exchanger are obtained.

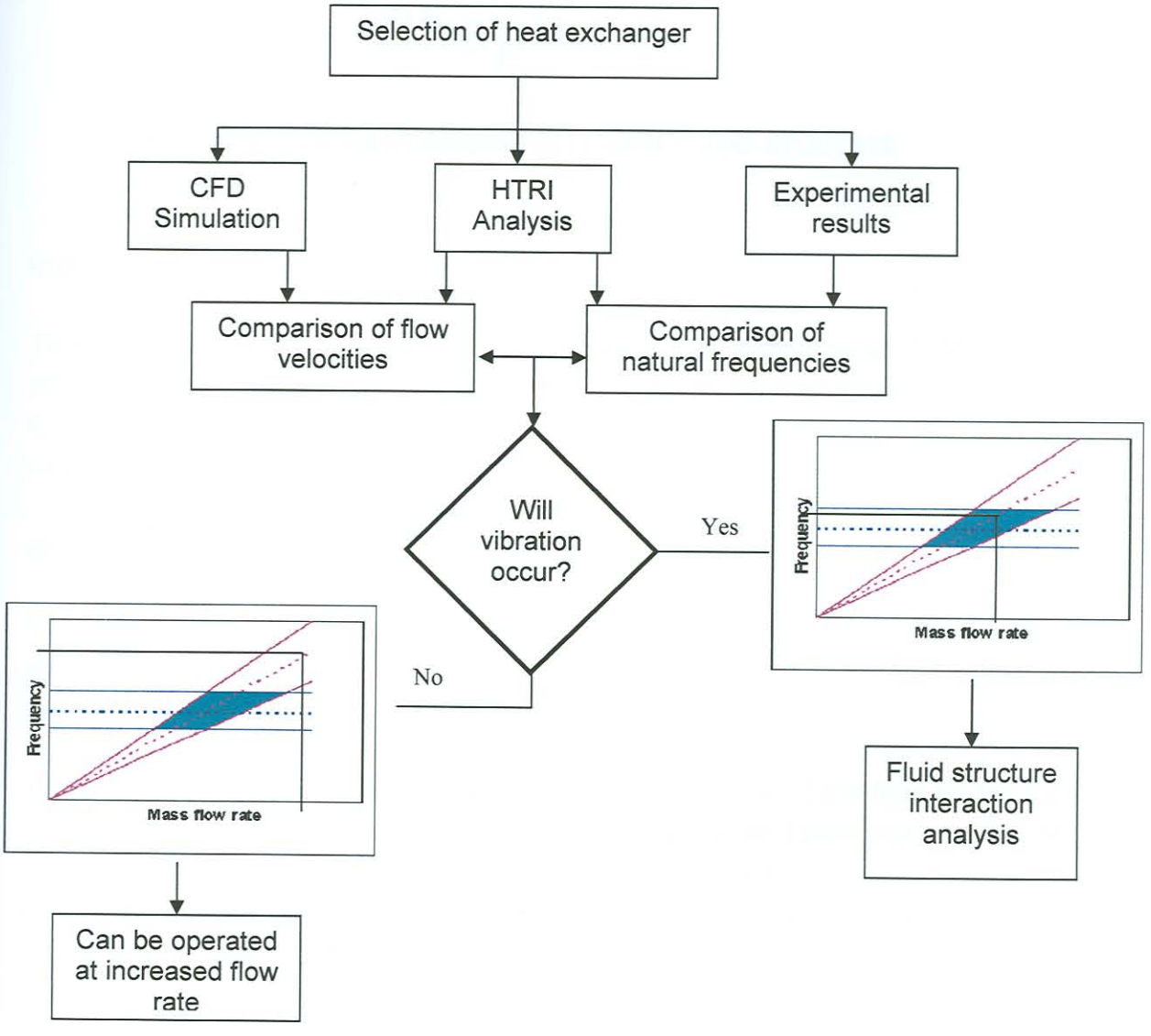

Figure 1.11: Research methodology diagram

Vibration measurements on the selected exchanger at normal loads and at increased loads were taken. The measuring procedure and experimental results are given in Chapter 4. In Chapter 5 the HTRI results, CFD results and experimental results are compared. The margins of uncertainty in the predicted values are also described. Chapter 6 contains the conclusion and recommendations from the research study.